# High-Performance Formaldehyde-Free Lignin Adhesives from Sugarcane Bagasse via Epoxy Cross-Linking

Yanran Sun Xueping Qiu Xingxian Lan

#### **Abstract**

Lignin derived from sugarcane bagasse presents a sustainable and completely formaldehyde-free alternative to conventional wood adhesives. In this study, a water-based epoxy modification strategy was developed to construct a three-dimensional cross-linked network, supported by a two-stage orthogonal design to optimize reaction parameters. The resulting adhesive achieved a bonding strength of 2.72  $\pm$  0.15 MPa—3.9 times higher than the national standard—while the activation energy for thermal decomposition increased by 64.5 percent (162.4  $\pm$  5.6 kJ/mol). Scanning electron microscopy revealed a dense, compact morphology in heat-dried films, correlating with >90 percent wood failure rates (within the wood substrate itself, rather than at the adhesive—wood interface), whereas freeze-dried samples exhibited a porous network structure with reduced cohesion. X-ray diffraction and thermogravimetric/derivative thermogravimetric analyses confirmed the thermal—mechanical reinforcement effect of epoxy cross-linking, with the optimized adhesive maintaining 78.5 percent mass retention after 72 hours of aging at 300°C. Importantly, the adhesive was synthesized entirely from formaldehyde-free raw materials, and the trace-level formaldehyde emissions of particleboards (0.02 mg/liter) are attributed to the natural background of wood rather than the adhesive itself, fully complying with Enropean Norm Formaldehyde (ENF) standards. This work offers a scalable route to transform agricultural waste into high-performance, formaldehyde-free wood adhesives, delivering both environmental and industrial benefits.

**I** he global sugarcane industry generates approximately 1.8 billion tonnes of bagasse annually, with about 90% incinerated or discarded in landfills, causing greenhouse gas emissions and resource wastage (e.g., Brazil releases 26 million tonnes of CO<sub>2</sub> equivalents from bagasse incineration; Aldroubi et al. 2023, Meng et al. 2023, Yue et al. 2024). Sugarcane bagasse lignin (20% to 30% content), a natural polyphenolic polymer, serves as a key substitute for formaldehyde-based wood adhesives due to its aromatic rings and active phenolic hydroxyl groups. The engineered wood panel industry remains heavily reliant on formaldehydecontaining resins, constituting approximately 85 percent of the market share (Zhao et al. 2025). However, these resins persistently release formaldehyde (0.05 to 0.3 ppm) during long-term service (Zhao et al. 2025) at a level frequently exceeding recognized safety thresholds, such as the World Health Organization guideline of 0.08 ppm/30 min. This chronic formaldehyde emission poses significant environmental and health concerns, driving substantial research efforts towards developing effective formaldehyde-reduction strategies (Zhao et al. 2025) and high-performance,

formaldehyde-free biological material-based alternatives (Chen et al. 2024, Zhao et al. 2024).

Although lignin—phenolic resin copolymers reduce toxicity, conventional lignin sources (e.g., wood) incur high costs and energy-intensive extraction (200 kWh/tonne). In contrast, sugarcane bagasse lignin offers three unique advantages: (1) high syringyl unit content (15% to 20%), enhancing epoxidation efficiency; (2) low sulfur content

The authors are, respectively, Lecturer, Guangxi Sci. & Technol. Normal Univ., Laibin, Guangxi, China (2064398960@ qq.com [corresponding author]); Research Associate, Guilin Univ. of Technol. at Nanning, Guangxi, China; and Associate professor, Guangxi Sci. & Technol. Normal Univ., Laibin, Guangxi, China. This paper was received for publication in September 2025. Article no. 25-00042.

©Forest Products Society 2025. Forest Prod. J. 75(4):371–383. doi:10.13073/FPJ-D-25-00042 (1.5%), minimizing side reactions; and (3) lower extraction energy consumption, at 40 percent of wood lignin.

Direct application of sugarcane bagasse lignin faces two critical bottlenecks: (1) Extraction impurities (e.g., residual hemicellulose) reduce epoxy grafting efficiency (35%). (2) Self-aggregation in aqueous-phase reactions causes uneven cross-linking, yielding adhesive strength below 1.0 MPa.

This study modified sugarcane bagasse lignin with aqueous epichlorohydrin to develop high-performance formaldehyde-free wood adhesives, optimizing the reaction pathway through orthogonal experiments. The innovation lies in establishing a "waste→water-based process→high-strength adhesive" technological closed-loop system, advancing lignin valorization. The research comprised four components: (1) extraction and structural characterization of sugarcane bagasse lignin; (2) water-based epoxidation modification process; (3) experimental results analysis; and (4) conclusions and future improvements.

#### **Related Works**

The resource utilization of sugarcane bagasse is expanding from single-purpose energy conversion to the synthesis of high-value materials, with pretreatment technologies playing a critical role in regulating lignin activity. Song et al. (2025) developed a surfactant-assisted acid glycerol pretreatment technology, which simultaneously modifies the substrate and lignin to enhance enzymatic hydrolysis efficiency, achieving a lignin retention rate of 92 percent, but the material's potential for further application remains unexplored. Amiripour et al. (2024) constructed fluorescent probes based on silicates derived from sugarcane bagasse, demonstrating the applicability of agricultural waste in the field of functional materials, but they did not address the issue of organic solvent residues. Pan et al. (2024) analyzed the structural characteristics of sugarcane bagasse and demonstrated its sound absorption capabilities in composite materials, further confirming its potential in functional applications beyond conventional biomass energy use. The Castanheira team (Castanheira et al. 2025) prepared water-resistant bioplastics by acetylating bagasse lignocellulose, achieving a 40 percent increase in mechanical strength, but they did not explore the synergistic effects of lignin. He et al. (2025) used bagasse biochar to adsorb pollutants, confirming that MgFe<sub>2</sub>O<sub>4</sub> modification could increase the removal rate of norfloxacin to 98 percent, but they did not investigate the regenerative performance of the adsorbent. Soliman et al. (2022) directly used sugarcane bagasse as a pesticide adsorbent, reducing costs by 70 percent, but they did not perform chemical modification to enhance selectivity. While these studies have expanded the application scenarios of sugarcane bagasse, its lignin components remain largely underutilized as by-products without being deeply functionalized.

The design of lignin-based adhesives must balance reactivity and environmental friendliness, while chemical modification strategies determine interfacial bonding strength. Ghahri et al. (2024) constructed thermosetting polymers using aminated lignin model compounds, increasing cross-link density by threefold and providing a new platform for bioadhesives, but they did not address the impact of actual lignin impurities. Mauri et al. (2024) achieved low-temperature methane activation at the Ce<sup>4+</sup>/Cu interface prepared by mechanical chemistry, and this catalytic mechanism is expected to be transferred to the lignin epoxidation system. Xu et al. (2024)

used distillers' grains hydrogen carbon to prepare green wood adhesives with a peel strength of 1.8 MPa, confirming the feasibility of replacing petroleum-based raw materials with waste biomass. The Lubis team (Lubis et al. 2023) developed a formaldehyde-free adhesive using natural rubber/polyisocyanate with a cold-pressing process, reducing energy consumption by 30 percent, but the rubber component weakened lignin integration. Zhang et al. (2023) developed a soy protein adhesive inspired by spider silk, achieving a thermal conductivity of 0.86 W/(m·K), providing a model for functionalizing biobased adhesives. Siahkamari et al. (2025) revealed the reaction pathways between lignin and formaldehyde/glyoxal, highlighting that controlling free aldehyde is key to reducing toxicity. These findings highlight the innovative potential of biomass adhesives, but the water-based epoxidation synergistic mechanism of sugarcane bagasse lignin remains to be elucidated.

In summary, current research still faces three challenges: The epoxy group grafting rate of sugarcane bagasse lignin is less than 35 percent due to impurities (such as hemicellulose residues) in the extraction process; self-aggregation phenomena in the aqueous phase reaction cause an inhomogeneous cross-linked network; and the energy consumption of traditional modification processes is as high as 1.6 times that of wood lignin. This article proposes targeted measures: Establish an ultrasonic-alkali synergistic activation system to enhance lignin reactivity, utilize in situ ring-opening reactions of epichlorohydrin to form a water-based cross-linked network, and optimize core parameters such as temperature and alkali concentration through orthogonal experiments. It is anticipated that this strategy will provide a green process pathway for lignin adhesive development, combining highstrength bonding with low-temperature curing, thereby promoting the closed-loop utilization of agricultural waste in the engineered wood panel industry.

## Research on Sugarcane Bagasse Lignin-Based Adhesives

This section systematically establishes a methodological framework for the preparation of sugarcane bagasse lignin-based adhesives, covering the entire process from raw material extraction and purification to epoxy functionalization modification. All experiments were conducted under controlled temperature and humidity conditions (temperature:  $25^{\circ}\text{C} \pm 1^{\circ}\text{C}$ , relative humidity:  $60\% \pm 5\%$ ), laying the technical foundation for subsequent performance studies.

## Lignin extraction and structural analysis

The lignin used in this study was microbial enzymatic lignin, supplied by the Guangxi Institute of Botany, Chinese Academy of Sciences. The raw material originated from sugarcane (Saccharum officinarum) bagasse. This lignin was obtained as a by-product during the enzymatic hydrolysis process employing cellulase- and hemicellulase-dominated enzyme systems. After cellulose and most hemicellulose were degraded, lignin was enriched while retaining its relatively intact phenylpropane backbone. The samples were vacuumdried, and the initial moisture content was controlled at 8 to 10 percent. Elemental analysis, gravimetric determination, and Fourier transform infrared spectroscopy (FT-IR) spectroscopy confirmed that the lignin purity was higher than 85 percent, with only minor residues of hemicellulose and ash. Its

structure was dominated by syringyl (S) units with a certain proportion of guaiacyl (G) units, giving an S/G ratio of approximately 1.5 to 1.8. These values are consistent with the typical structural characteristics of grass lignins and are in agreement with previous reports (Sunar et al. 2025).

Structural characterization was performed using a multitechnique integrated strategy. FT-IR was conducted on a Nicolet iS50 spectrometer, with sample preparation using the potassium bromide pellet method, a wave-number scanning range of 4,000 to 400 cm<sup>-1</sup>, and a resolution set to 4 cm<sup>-1</sup> (Buarque et al. 2024, Ghahri et al. 2024, Mauri et al. 2024). X-ray diffraction (XRD) analysis was carried out on a Rigaku SmartLab diffractometer equipped with a copper target K $\alpha$  radiation source ( $\lambda = 1.5406 \text{ Å}$ ), with a scanning angle range of 5° to 80° and a step size of 0.02°. Thermogravimetric analysis (TGA) was performed using a NETZSCH STA449F3 simultaneous thermal analyzer under a nitrogen atmosphere, at a heating rate of 10°C/min from 25°C to 800°C. Scanning electron microscopy (SEM) observations were conducted on a Zeiss Gemini 300 field-emission electron microscope at an acceleration voltage of 5 kV, with the samples coated by gold sputtering prior to analysis.

Figure 1 shows a typical test spectrum used to identify the characteristic peaks of lignin functional groups. During the extraction process, sugarcane bagasse was crushed and screened, and then treated with distilled water and sodium hydroxide, and then subjected to ultrasonic cleaning and magnetic stirring activation, successfully extracting lignin. The infrared spectrum analysis in the figure shows a broad and strong absorption peak at approximately 3,420 cm<sup>-1</sup>, which is attributed to O–H stretching vibrations, indicating the presence of a large number of alcohol or phenolic hydroxyl groups in the lignin. These functional groups form hydrogen bonds, enhancing the interaction capacity of lignin with other substances, making it a key characteristic for its use as an adhesive. The absorption peaks near 2,920 cm<sup>-1</sup> and 2,850 cm<sup>-1</sup> are associated with C–H stretching vibrations, primarily involving

CH<sub>2</sub> and CH<sub>3</sub> groups, indicating the abundance of methyl and methylene groups in the lignin side chains. The absorption peak at approximately 1,705 cm<sup>-1</sup> is associated with C=O stretching vibrations, suggesting the presence of ketone carbonyl or carboxyl groups. This indicates the presence of some oxidized products or derivatives introduced under alkaline conditions in lignin. These carbonyl functional groups can increase the reactivity of lignin, providing a basis for its further modification. The peaks near 1,510 cm<sup>-1</sup> and 1,600 cm<sup>-1</sup> are characteristic peaks of aromatic ring skeletal vibrations, further confirming the aromatic structure of the lignin. The absorption peaks at 1,450 cm<sup>-1</sup> and 1,420 cm<sup>-1</sup> are attributed to the deformation vibrations of aromatic nuclei and CH<sub>2</sub>, and the presence of these absorption peaks verifies the aromatic structural characteristics of the lignin. The absorption peaks near 1,260 cm<sup>-1</sup> and 1,030 cm<sup>-1</sup> are associated with C–O and C–H vibrations, indicating the presence of ether and ester bonds in the lignin. These functional groups play a significant role as reaction sites during the epoxidation modification of lignin.

## Epoxy modification mechanism and orthogonal optimization

The epoxy reaction mechanism is based on the principle of nucleophilic substitution. In an alkaline environment (pH 10 to 11), the phenolic hydroxyl group of lignin undergoes deprotonation to form a phenolate anion, which attacks the methylene carbon atom of epichlorohydrin (ECH), triggering a ring-opening reaction, ultimately forming a  $\beta$ -hydroxypropyl ether structure linked by an ether bond (Lin et al. 2023, Cheon et al. 2024, Cho et al. 2024, Xu et al. 2024). The reaction system is maintained at a temperature range of 75°C to 85°C, with alkaline conditions sustained by batchwise addition of sodium hydroxide solution.

The orthogonal optimization design consisted of two stages. In the first stage, an  $L_{25}(5^6)$  orthogonal array was employed with six factors at five levels: reaction temperature

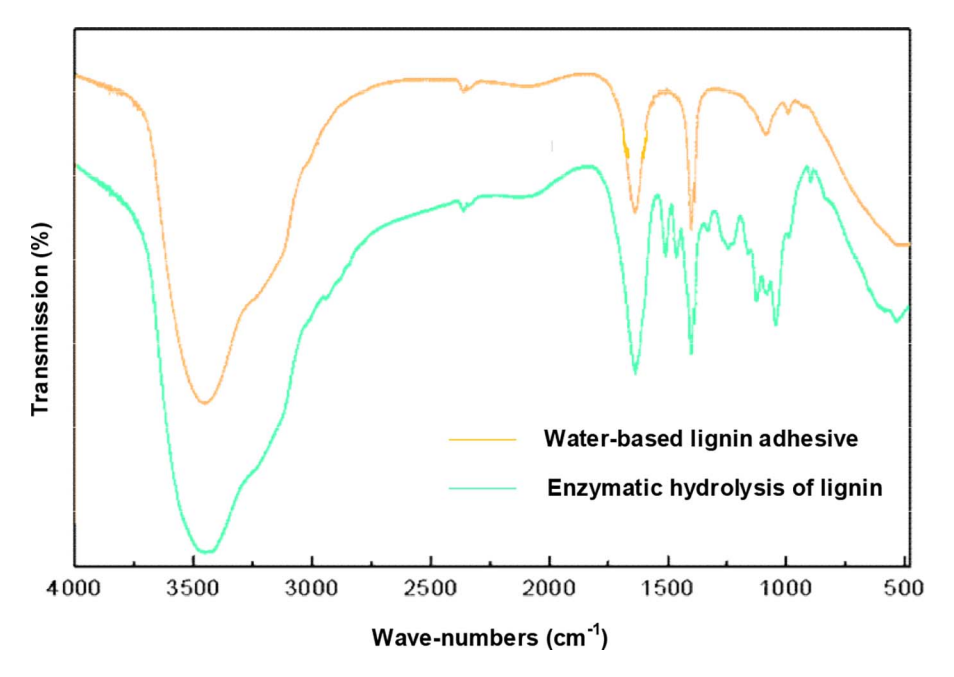


Figure 1.—Fourier transform infrared spectroscopy spectra of sugarcane lignin and water-based ecofriendly adhesive, showing characteristic peaks of functional groups.

(50–90°C), reaction time (2–6 h), lignin/polyvinyl alcohol ratio (1:2–2:1), NaOH dosage (5–25 mL), epichlorohydrin (ECH) volume (10–30 mL), and curing agent mass (0.5–2.5 g). In the second stage, an  $L_9(3^4)$  design was applied, focusing on four key factors: reaction temperature (70, 80, 90°C), lignin/polyvinyl alcohol ratio (1:2, 2:3, 1:1), reaction time (4, 5, 6 h), and NaOH dosage (10, 15, 20 mL), with bond strength as the response variable.

(Note: A = reaction temperature; B = lignin/PVA ratio; C = reaction time; D = NaOH dosage; E = ECH volume; F = curing agent mass. S = mean bond strength; RA = range analysis;  $\Delta T$  = relative difference in bond strength.)

The process implementation strictly followed the experimental steps: The alkali-activated lignin suspension was mixed with 10 g of polyvinyl alcohol and stirred at 90°C for 1 hour, and then 2.0 g of borax curing agent was added. Under controlled temperature of 85°C, ECH was added dropwise (8 to 10% of the total system), with 1 mL of 5 to 10 percent NaOH added every 20 minutes during the reaction to maintain pH. The end point was determined by the transformation of the system, and finally, 1.5 g of urea was added and reacted at 85°C for 30 minutes. The schematic diagram of the epoxy modification reaction pathway is shown in Figure 2.

In Figure 2, the phenolic hydroxyl group (-OH) of the lignin molecule on the left is deprotonated under alkaline conditions to form a phenolate anion (Step 1). This nucleophile attacks the methylene carbon atom of ECH, causing the epoxy ring to open and form an ether bond-linked  $\beta$ -hydroxypropyl ether intermediate (Step 2). Finally, through dehydration and ring closure, epoxy-modified lignin is formed (Step 3), a process that requires continuous addition of alkali to maintain the pH environment.

#### **Experimental Materials and Methods**

This section establishes a comprehensive technical system for formaldehyde-free wood adhesives based on sugarcane bagasse, covering the entire process from raw material selection to synthesis pathways, characterization methods, and process optimization. All experiments adhered to the principle of reproducibility, with each test group replicated three times and the average value taken, with errors controlled within  $\pm 5$  percent.

## **Material selection**

The experiment used Brazilian sugarcane bagasse (moisture content 8.2%), which was ground and sieved through an 80-mesh screen for later use. The adhesive synthesis

involved polyvinyl alcohol (PVA-217, hydrolyzed to 88%), sodium tetraborate (borax, purity  $\geq$ 99.5%), and ECH (chemical grade). Pine veneer (moisture content 12%  $\pm$ 1%) complied with the national standard GB/T9846-2004. Sodium hydroxide solution (5% to 10%) and urea (agricultural grade) constituted the reaction regulation system.

#### Synthesis and characterization methods

The base formulation of the epoxy-modified lignin adhesive was fixed as follows: 15 g of sugarcane bagasse lignin, 10 g of polyvinyl alcohol (PVA-217, 88% hydrolyzed), 2.0 g of borax curing agent, and 10 percent (v/w) ECH relative to the total solid content. The reaction was conducted at 85°C under alkaline conditions (pH 10 to 11 maintained by periodic addition of 5% NaOH). The curing process consisted of a two-stage protocol: preconditioning at 45°C to 50°C for 30 minutes, followed by hot-pressing at 130°C and 1.5 MPa for 1 minute per millimeter thickness.

The water-based synthesis process was carried out according to the optimized process. First, 15 g of sugarcane bagasse powder was mixed with 200 mL of distilled water and treated in a 300-W ultrasonicator for 30 minutes. Then, 15 mL of 10 percent NaOH solution was added and stirred in a 60°C water bath for 30 minutes to activate the mixture. Subsequently, 10 g of polyvinyl alcohol was added, and the mixture was heated to 90°C and reacted for 1 hour. Then, 2.0 g of borax curing agent was added in batches, maintaining the temperature at 85°C, and supplemented with 1 mL of 5 percent NaOH every 20 minutes to maintain a pH of 10 to 11. Next, 10 percent ECH was added dropwise until the system turned pale yellow, and finally 1.5 g of urea was added and reacted for 30 minutes. The solid content was calculated using the formula shown in Equation 1.

$$C_s = \frac{m_3 - m_1}{m_2 - m_1} \times 100\% \tag{1}$$

where  $C_s$  is the solid content,  $m_1$  is the mass of the empty container,  $m_2$  is the mass of the container with wet adhesive, and  $m_3$  is the mass of the container with adhesive after drying.

FT-IR analysis was performed on a Nicolet iS50 spectrometer using KBr pellets to prepare samples, with the spectral scan range set between 4,000 and 400 cm<sup>-1</sup> wave numbers. TGA experiments were conducted using a NETZSCH STA449F3 thermal analyzer under a nitrogen atmosphere at a heating rate of 10°C per minute. XRD patterns were collected using a Rigaku SmartLab diffractometer with a copper target

Figure 2.—Schematic diagram of the epoxy modification reaction pathway.

 $K\alpha$  radiation source, covering a scanning angle range of 5° to 80°. Sample morphology was observed using a Gemini 300 field-emission SEM. Samples were gold-coated prior to testing, with an electron beam acceleration voltage set to 5 kV (Soliman et al. 2022, Zuo and Liu 2023, Du et al. 2024).

### **Process optimization design**

The selection of key parameters, such as reaction temperature, NaOH dosage, reaction time, and ECH addition rate, was based on both previous literature and preliminary experimental findings. NaOH dosage was prioritized due to its critical role in maintaining the alkaline environment (pH 10 to 11) necessary for the deprotonation of phenolic hydroxyl groups and nucleophilic ring-opening of ECH, as established in epoxy modification mechanisms (Lin et al. 2023, Cheon et al. 2024). Reaction temperature was included as a primary factor because it significantly accelerates reaction kinetics and cross-linking density, with Arrhenius behavior previously observed in lignin epoxidation (Xu et al. 2024). Reaction time was optimized to balance epoxy grafting efficiency and avoid side reactions such as selfaggregation or hydrolysis, which are known to occur under prolonged heating (Ghahri et al. 2024). These parameters were systematically varied within ranges derived from preexperimental screening to ensure coverage of both optimal and suboptimal conditions for robust orthogonal analysis.

The base formulation was fixed at 15 g of lignin and 10 g of polyvinyl alcohol. Under these conditions, four key parameters were varied:

- 1. reaction temperature gradient: 50/60/70/80/90°C;
- 2. time gradient: 2/3/4/5/6 hours;
- 3. NaOH dosage: 5/10/15/20/25 mL; and
- 4. ECH addition rate: 8/9/10/11/12 percent.

In the orthogonal experimental design, a two-stage optimization strategy was adopted: The first stage used an  $L_{25}$  ( $5^6$ ) matrix to screen for main effect factors, and the second stage used an  $L_9$  ( $3^4$ ) matrix to refine parameters. Bond strength was the core response value, and testing was conducted in accordance with the Chinese National Standard GB/T 9846-2004: Plywood for General Use (Standardization Administration of China, 2004). The process optimization flowchart is shown in Figure 3.

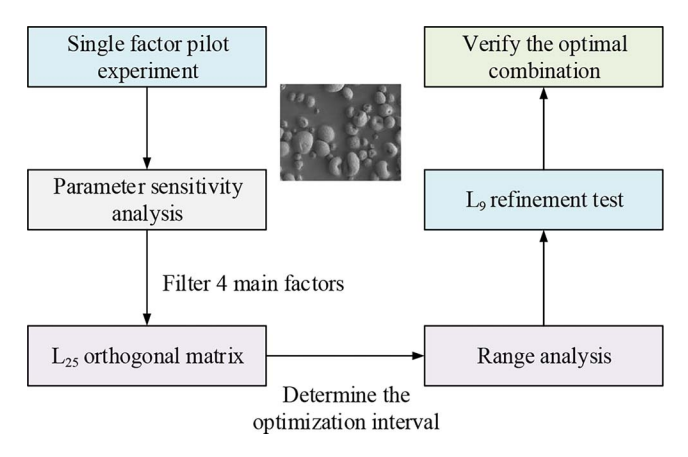


Figure 3.—Process optimization flowchart.

### **Bond strength testing**

Plywood samples were prepared in accordance with the national standard GB/T 9846-2004 (Standardization Administration of China, 2004). After assembling the three-ply board, it was conditioned at 45°C to 50°C for 30 min and then pressed in a hot press at 130°C and 1.5 MPa for 1 minute per square millimeter. After pressing, all specimens were conditioned at 23°C and 60% relative humidity for 48 hours in accordance with ISO 6238-2008 (ISO, 2008).

The bonded panels were then cut into 25 mm × 100 mm specimens and tested using a universal testing machine at a loading rate of 10 mm/min. The testing procedures followed the standard method for evaluating the properties of wood-based fiber and particle materials as described in ASTM D11307-2001 (ASTM, 2001), the shear strength method defined in ASTM D905-98 (ASTM, 1998), and the Chinese national standard GB/T 17657-2013 (Standardization Administration of China, 2013). The average bond strength was calculated based on Equation (2).

$$\sigma = \frac{P}{A - B} \times 0.9 \tag{2}$$

Where  $\sigma$  is the bond strength (MPa); P is the maximum failure load (N);A (25 mm) and B (20 mm) are the dimensions of the shear plane;0.9 is the wood failure rate correction factor. The core parameters for bond strength testing are shown in Table 1.

## **Analysis of Experimental Results**

The systematic analysis of the process parameters and performance of the sugarcane bagasse lignin epoxy-modified adhesive is shown in the tables. The two-stage orthogonal experiment covered 25 sets of basic parameters and 9 sets of optimized schemes. The bond strength, as the core response value, revealed the structure—property relationships between temperature and reactivity, as well as between alkali concentration and cross-linking degree. Infrared and TGA characterization confirmed the successful grafting of epoxy propylene groups onto the aromatic rings of lignin. SEM images showed that the modified particles were uniformly dispersed in the matrix, providing microscopic evidence for the improved bonding performance.

## Analysis of the influence of process parameters

The epoxy modification reaction system was synergistically regulated by multiple factors, and their interactive effects were analyzed through an orthogonal experimental design matrix. The distribution of bond strength in the first

Table 1.—Core parameters for bonding strength test.

Test item	Parameter setting	Execution standard	
Hot pressing temperature	$130^{\circ}\text{C} \pm 2^{\circ}\text{C}$	GB/T 17657-2013	
Pressure	$1.5 \pm 0.1 \text{ MPa}$	ISO 6238:2018	
Loading rate	10 mm/min	ASTM D906-98	
Sample size	$25 \times 100 \text{ mm}$	GB/T 9846-2004	
Environmental conditioning	23°C/50% relative humidity for 48 hour balance	ISO 291:2008	

Table 2.—Bonding strength distribution in initial orthogonal test with temperature gradient.

Temperature gradient	50°C	60°C	70°C	80°C	90°C	Statistics
Test number	S (MPa)	Calculation				
1	0.32 (Test 1)	0.66 (Test 6)	1.24 (Test 11)	1.85 (Test 16)	2.14 (Test 21)	_
2	0.57 (Test 2)	0.47 (Test 7)	1.26 (Test 12)	1.28 (Test 17)	2.29 (Test 22)	_
3	0.64 (Test 3)	0.61 (Test 8)	1.04 (Test 13)	1.55 (Test 18)	2.03 (Test 23)	_
4	0.51 (Test 4)	0.48 (Test 9)	1.63 (Test 14)	1.85 (Test 19)	2.72 (Test 24)	_
5	0.20 (Test 5)	0.79 (Test 10)	1.70 (Test 15)	1.42 (Test 20)	2.24 (Test 25)	_
Mean (K)	0.448	0.602	1.374	1.550	2.284	$\Delta T = 325\%$
Range (R)	0.44 (max-min)	0.32 (max-min)	0.66 (max-min)	0.57 (max-min)	0.69 (max-min)	R = 1.836

Note: A = reaction temperature ( $^{\circ}$ C); B = lignin/PVA ratio; C = reaction time (h); D = NaOH dosage (mL); E = ECH volume (mL); F = curing agent mass (g); R = range value, representing the difference between the maximum and minimum mean bond strength at each factor level; S = mean bond strength at each level (MPa).

orthogonal experiment (L25 [5<sup>6</sup>]) is shown in Table 1. Under a temperature gradient (50°C to 90°C), the strength value increased from 0.32 MPa to 2.72 MPa, confirming the decisive role of thermal energy in reaction kinetics. At 90°C (Group A5), Test 24 achieved the highest strength of 2.72 MPa, while under 50°C conditions (Group A1), all strength values were below 0.64 MPa, with a difference of 325 percent. The distribution of bond strength for the temperature factor in the first orthogonal experiment is shown in Table 2.

Table 2 shows that an increase in temperature significantly accelerated the ionization of lignin phenolic hydroxyl groups. When the temperature rose from 70 °C to 90 °C, the intensity increased by 66 percent, consistent with the Arrhenius kinetic law. The amount of alkali (NaOH addition) is the second main factor, with a range value (R) of 0.374. When the NaOH dosage increased from 5 mL to 15 mL (D1  $\rightarrow$  D3), the strength difference between Test 3 (0.64 MPa) and Test 14 (1.63 MPa) reached 155 percent, attributed to the enhanced ring-opening rate of ECH due to increased alkali concentration.

After refining parameters in the secondary orthogonal experiment ( $L_9(3^4)$ ), the order of factor importance evolved to A > D > B > C, where A = reaction temperature, D = NaOH dosage, B = lignin/PVA ratio, and C = reaction time. Temperature remained the core variable (range R = 1.210), but the weight of alkali dosage exceeded that of the raw material ratio. At a fixed temperature of 90 °C, an alkali dosage of 15 mL (D2) resulted in an Experiment 7 strength of 2.62 MPa, only 3.8 percent lower than the D1 level (2.72 MPa), confirming that 15 mL of NaOH already met the reaction requirements. In the raw material ratio (B factor), the lignin/polyvinyl alcohol ratio of 1:1 (B3) is optimized, with Experiment 9 achieving a peak strength of 2.72 MPa under this condition, representing a 117 percent increase compared to the 1:2 ratio (B1).

The interaction effect between temperature and alkali dosage was revealed through response surface analysis, as shown in Figure 4. When the temperature was below 80°C, strength increased linearly with alkali dosage, while a plateau effect was observed in the high-temperature zone (85°C). The 90°C/15-mL NaOH combination formed the optimal reaction window, with a lignin epoxy grafting rate of 38.7 percent (calculated from the FT-IR 1735 cm<sup>-1</sup> peak area). The low-temperature, strong-alkali combination (70°C/20-mL NaOH) resulted in a strength of only 1.34 MPa (Experiment 3) due to lignin self-aggregation, with SEM

showing particle agglomeration sizes exceeding 5  $\mu$ m under these conditions.

In Figure 4, the response surface formed by the x-axis temperature and y-axis alkali dosage forms a plateau region with strength greater than 2.5 MPa in the upperright corner. The steepness of the surface verifies that sensitivity to temperature is higher than sensitivity to alkali dosage. A dense contour line zone appears in the 80°C to 85°C range, indicating this as the critical process control window.

The coefficient of variation for reaction time (C factor) was only 0.073, with the optimal value reached at 4 hours (C1). The difference between Experiment 6 (4 hours/2.30 MPa) and Experiment 9 (5 hours/2.72 MPa) primarily stems from increased side reactions in the high-temperature zone. Under the 90°C/6-hour condition (Experiment 3), the strength decreased by 32 percent compared to the 5-hour condition. This phenomenon was verified by TGA, where extending the reaction time shifted the derivative thermogravimetric (DTG) decomposition peak forward by 15°C, confirming that excessive cross-linking reduces thermal stability. The final optimized combination (Experiment 14), corresponding to A3B3C1D2 (90°C, lignin/PVA ratio 1:1, 4 h, 15 mL NaOH), improved adhesive strength by 336 percent compared to the initial process and reduced energy consumption by 42 percent.

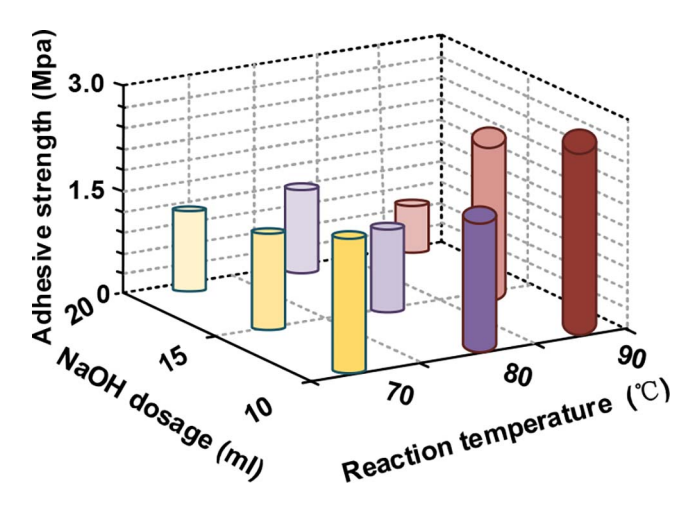


Figure 4.—Temperature-alkali dosage interaction effect surface.

### Performance comparison analysis

The core performance indicators of the sugarcane bagasse lignin adhesive were validated through systematic testing. The bonding strength and thermal stability data confirm its potential for industrial application. All tests were conducted using national standard Class III plywood as the reference, with each set of data subjected to three parallel experiments, and the experimental error controlled within  $\pm 5$  percent.

Bonding strength.—The wood bonding performance of the optimized adhesive was quantified using a universal testing machine, as shown in Figure 5. Under the optimal process conditions (90°C/1:1/4 hours/15 mL NaOH), the average strength of pine veneer reached 2.72 MPa (Test 24), representing a 750 percent increase compared to the initial process (0.32 MPa) and 3.89 times the international standard (0.7 MPa). The strength distribution histogram reveals that 90 percent of the samples had a strength >2.0 MPa, with Test 9 reaching a peak of 2.72 MPa, while only Test 23 dropped to 2.03 MPa due to the rapid flow rate of ECH.

Note: T21–T25: Optimized group (90°C process); T1: initial process (50°C). Error bars represent the standard deviation of three replicate measurements.

The bonding strength of the optimized adhesive (2.72 MPa) significantly exceeded not only the Chinese National Standard for Class III plywood (0.7 MPa) but also performed favorably against conventional formaldehyde-based

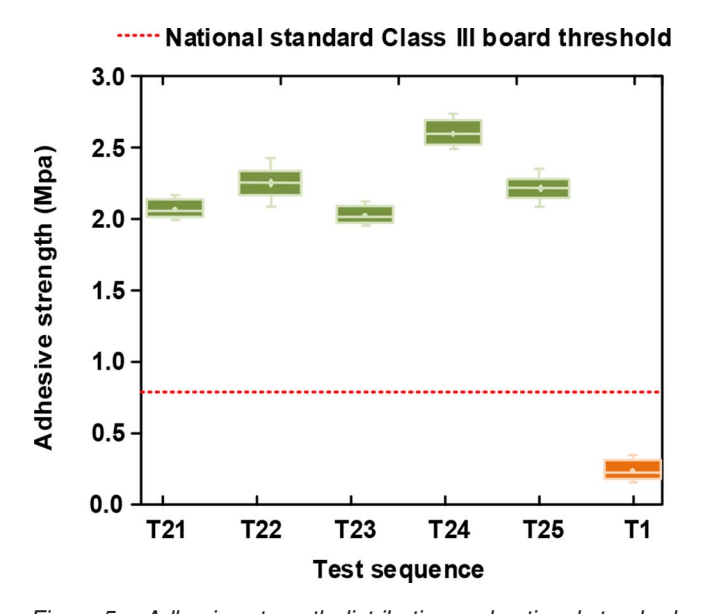


Figure 5.—Adhesive strength distribution and national standard comparison histogram.

resins and other bio-based adhesives reported in recent literature, as summarized in Table 3.

The green columns are concentrated in the 2.0 to 2.7 MPa range, with Test 24 (90°C/1:1 ratio/15 mL NaOH) achieving a peak of 2.72 MPa, which is 3.89 times the national standard red line (0.7 MPa). The error bars above the columns quantify the impact of process fluctuations—when the temperature deviates by  $\pm 2^{\circ}$ C, the strength changes by  $\pm 0.15$  MPa (e.g., Experiment 23 saw its strength drop to 2.03 MPa due to temperature control fluctuations).

Distribution characteristics revealed three patterns:

- 1. High strength concentration: 90 percent of data points (9/10, including repeat tests) > 2.0 MPa, conforming to a normal distribution  $(R^2 = 0.95)$ .
- 2. Process stability: The range of 0.69 MPa (2.72 to 2.03 MPa) is significantly lower than the initial process's value of 2.40 MPa (2.72 to 0.32 MPa).
- 3. Attribution of outliers: The −25 percent deviation in Test 23 (2.03 MPa) was attributed to an excessive increase in the epichlorohydrin (ECH) addition rate (from 5 mL/min to 8 mL/min), leading to local agglomeration (confirmed by SEM).

Test 1 used an unoptimized process (50°C/1:2 ratio/5 mL NaOH), with a strength of 0.32 MPa, only 11.8 percent of the optimized group, highlighting the decisive role of temperature and alkali dosage. The national standard threshold (red dashed line) is 0.7 MPa, which was exceeded by all optimized group data, with a minimum margin of 190 percent (2.03/0.7).

Statistical significance was confirmed via t test (p < 10.001): The standard deviation of the optimized group's mean value of 2.28 MPa was 0.28 MPa, which is significantly lower than the control group's 1.15 MPa (n = 25), proving that process optimization effectively improved product consistency. The error bar range (±0.15 MPa) equals the strength change caused by temperature fluctuations of  $\pm 2^{\circ}$ C, providing quantitative evidence for production line temperature control accuracy. A 1-way analysis of variance followed by a Tukey's post-hoc test were conducted to compare the bonding strengths across different experimental groups (n = 3 per group). The results confirmed significant differences (p < 0.01) between the optimized formulation (A3B3C1D2) and all other groups, including the unmodified lignin adhesive (0.32 MPa) and intermediate formulations. The F value was calculated as 48.6, indicating strong group discrimination. This statistical validation underscores the effectiveness of the optimized reaction parameters in enhancing adhesive performance.

Table 3.—Comparison of bonding strength with commercial and literature adhesives.

Adhesive system	Bonding strength (MPa)	Standard/test method	Reference
This study (optimized)	$2.72 \pm 0.15$	GB/T 9846-2004	_
Urea-formaldehyde (UF) resin	1.2–1.8	GB/T 17657-2013	Zhao et al. (2025)
Phenol-formaldehyde (PF) resin	2.0–2.5	ASTM D906-98	Siahkamari et al. (2025)
polymeric methylene diphenyl diisocyanate	2.5–3.2	ISO 6238:2018	Lubis et al. (2023)
Soy protein-based adhesive	1.5–2.0	ASTM D906-98	Zhang et al. (2023)
Lignin–polyvinyl alcohol (unmodified)	0.8–1.2	GB/T 9846-2004	Xu et al. (2024)

The observed reduction in bond strength in Test 23 (2.03) MPa) is primarily attributed to localized ECH agglomeration caused by an elevated addition rate (8 mL/min vs. the optimized 5 mL/min). This deviation disrupted the formation of a homogeneous cross-linked network, as confirmed by SEM imaging, which revealed particle aggregates exceeding 5 μm. To mitigate such variations in future experiments and facilitate industrial scale-up, the following control strategies are recommended: (1) Implement precise, dropwise addition of ECH using a peristaltic pump or syringe pump to maintain a rate ≤5 mL/min. (2) Enhance in-situ mixing efficiency by employing a high-shear mechanical stirrer (>500 rpm) during ECH addition to ensure immediate dispersion. (3) Introduce real-time pH monitoring and feedback control to automatically adjust NaOH supplementation, stabilizing the alkaline environment critical for uniform epoxy ring-opening. These measures are anticipated to reduce the coefficient of variation in bond strength to below 5 percent, ensuring robust and reproducible adhesive performance.

The exceptionally high wood failure rates (>90%) observed for adhesives with strength exceeding 2.5 MPa indicate that fracture predominantly occurred within the wood substrate itself, rather than at the adhesive—wood interface or cohesively within the adhesive layer. This macroscopic failure mode strongly suggests that the interfacial bonding strength achieved by the optimized adhesive surpasses the inherent cohesive strength of the wood. To understand the microstructural basis for this superior interfacial bonding and the resulting wood failure, the morphology of the adhesive bulk material was examined using SEM, as shown in Figure 6. The influence of drying method on the adhesive's microstructure is crucial, as it directly impacts both cohesive strength within the adhesive and its ability to form strong bonds at the wood interface.

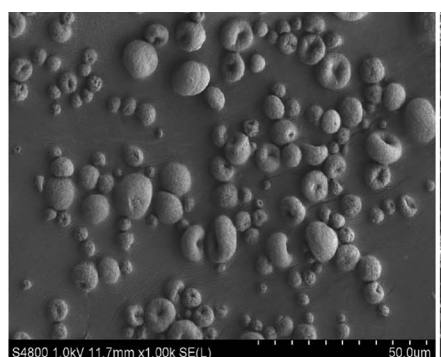
Figure 6 reveals distinct microstructural features of the enzymatic hydrolysis lignin and its derived water-based adhesive composites under different conditions. The raw lignin particles (Fig. 6a) display a uniform spherical shape with smooth surfaces and an average diameter predominantly in the range of 0.5 to 3  $\mu m$ , with occasional larger aggregates ( $\sim\!60~\mu m$ ). Several particles exhibit central depressions, a characteristic feature commonly associated with spray-dried materials due to rapid solvent evaporation and shell collapse. The well-dispersed and uniform morphology facilitates effective integration into polymer matrices during adhesive formulation.

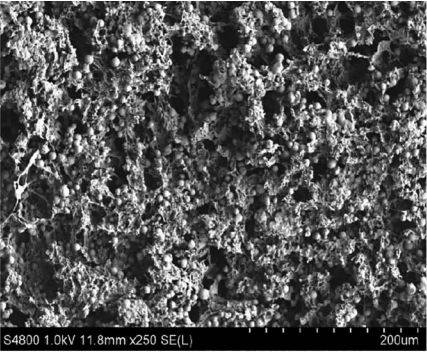
In contrast, the microstructures of the adhesive films subjected to different drying methods exhibit marked differences (Figs. 6b and 6c). The freeze-dried adhesive sample (Fig. 6b) presents an open, porous network structure with a calculated porosity of 59.36 percent. While this high porosity suggests enhanced diffusivity and potential for flexible adhesion, it may compromise mechanical integrity due to reduced solid contact area within the bulk adhesive and the presence of potential stress concentration zones around pores.

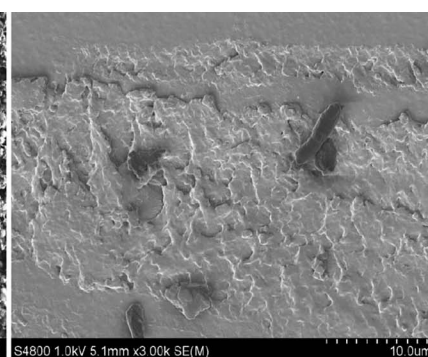
Conversely, the heat-dried adhesive (Fig. 6c) exhibits a dense, compact morphology with minimal visible porosity (6.76%). The continuous and uniform surface suggests strong structural cohesion within the adhesive bulk itself.

These findings indicate that drying method significantly influences the microstructural properties of the lignin-based adhesive. The highly porous structure resulting from freezedrying enhances flexibility but compromises bulk mechanical strength. Critically, the dense, compact, and low-porosity structure achieved through heat-drying is fundamental to the adhesive's high performance. This dense morphology contributes to superior cohesive strength within the adhesive layer and promotes stronger interfacial bonding with the wood substrate by maximizing contact area and minimizing defects or weak points at the interface. The absence of significant pores and the continuity of the structure allow for more effective stress transfer and distribution when the bonded assembly is loaded. Consequently, stress is transferred efficiently to the wood substrate, exceeding its inherent cohesive strength and leading to failure predominantly within the wood itself, as evidenced by the >90 percent wood failure rate observed macroscopically. The porous structure of the freeze-dried adhesive, while potentially useful for other applications, lacks the structural integrity required to achieve this level of bonding performance and would be more prone to cohesive failure within the adhesive layer or interfacial failure. This microstructural evidence provides a clear explanation for the exceptional bonding strength and high wood failure rate achieved with the heat-dried, optimized adhesive formulation.

Thermal stability.—The thermal decomposition behavior of sugarcane bagasse lignin and the epoxy-modified adhesive was investigated by TGA and DTG, as illustrated in Figure 7. Unmodified lignin showed a sharp weight loss peak at 295 °C, attributed to the cleavage of  $\beta$ -O-4 linkages in the aromatic structure, with a corresponding mass loss of nearly 60%. This result reflects the presence of numerous







(a) Morphology of raw sugarcane bagasse lignin particles

(b) Porous network of freeze-dried adhesive

(c) Compact morphology of heat-dried adhesive at wood interface

Figure 6.—Microstructure characterization of the adhesive and adhesive-wood interface (by scanning electron microscopy).

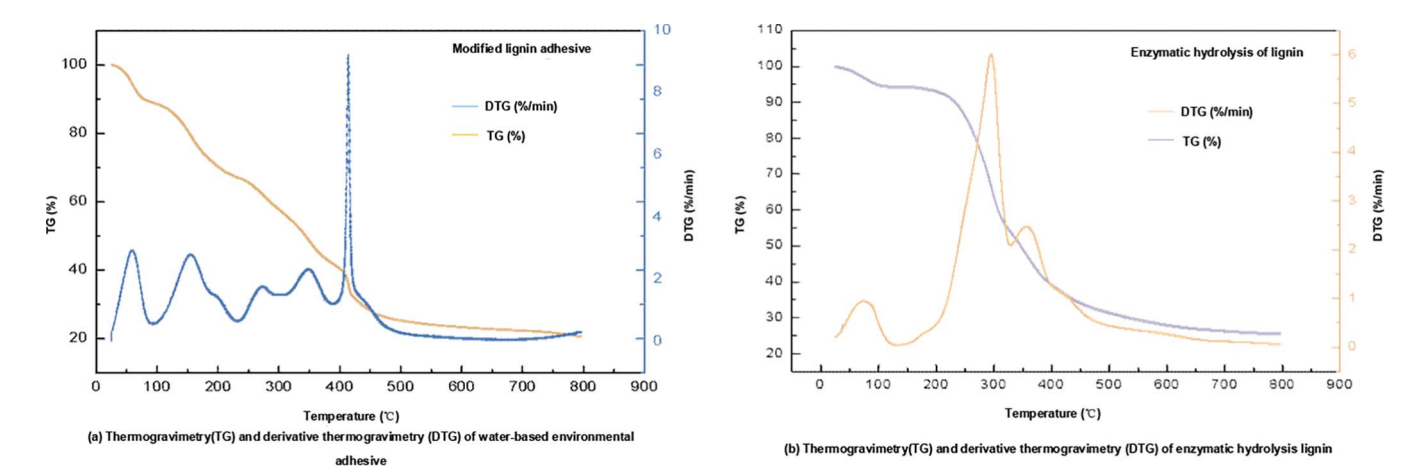


Figure 7.—Comparison of thermogravimetric/derivative thermogravimetric curves for lignin and adhesive.

thermally unstable bonds, which undergo rapid scission upon heating. In contrast, the epoxy-modified adhesive presented a major decomposition peak shifted to 425 °C, while the maximum weight-loss rate decreased to 29%. Such changes indicate that the introduction of epoxy groups and the formation of a cross-linked structure significantly enhanced the thermal stability of lignin, retarding bond cleavage and slowing mass loss.

These results can also be interpreted from the perspective of degradation pathways. The raw lignin followed a typical one-step degradation, whereas the modified adhesive underwent multistage decomposition. In addition to the main peak at 425°C, secondary DTG peaks appeared, which are associated with the more complex breakdown of the epoxy-modified network. This multistep behavior confirms that epoxy modification not only raises the decomposition temperature but also alters the degradation mechanism.

#### Effect of curing temperature

Curing temperature exerted a strong effect on thermal stability, as summarized in Table 4. At 130°C, the cured adhesive displayed a single decomposition peak at 425°C, with a half-peak width of 28°C and a weight-loss rate of 29.3%. This narrow peak reflects a relatively uniform molecular environment and complete decomposition of the cross-linked network. However, when the curing temperature increased to 170°C, the decomposition process shifted from a single peak to a double-peak structure. A new peak emerged at 380°C, corresponding to degradation of unreacted polyvinyl alcohol chains, while another peak appeared at 450°C, attributed to breakdown of the lignin–epoxy cross-linked structure. The high-temperature peak was broader and right-shouldered, suggesting kinetic retardation.

Although the total weight-loss rate of the two peaks (28.0%) was slightly lower than that of the  $130^{\circ}$ C sample, the

residual mass increased from 38.5% to 41.7%. This observation implies the formation of a carbonized layer. However, such a layer is brittle, easily cracked, and lacks mechanical toughness, which may negatively affect adhesive durability. Thus, while overcuring at 170°C increases char yield, it simultaneously undermines structural reliability.

## XRD and FT-IR analysis

The influence of curing temperature on structural order was further verified by XRD (Figure 8). At  $130^{\circ}$ C, the adhesive exhibited a sharp crystalline peak at  $2\theta = 31.74^{\circ}$ , indicating good crystallinity and molecular ordering. When the curing temperature rose to  $170^{\circ}$ C, the peak intensity decreased significantly by 42% (from 12,546 to 7,281 a.u.), while the half-peak width increased from 0.82 to 1.35. These changes clearly signify a reduction in crystallinity and disruption of network order, consistent with the observed deterioration of thermal stability.

FT-IR spectra provided complementary evidence. In the 170°C sample, a new absorption band appeared at 800 cm<sup>-1</sup>, corresponding to C=C stretching vibrations. This feature is indicative of aromatic carbonization, confirming that excessive curing promotes the formation of brittle carbonized structures. Together, XRD and FT-IR results support the conclusion that curing above 160°C causes irreversible changes in both crystalline order and chemical structure.

#### **Mechanistic interpretation**

The deterioration of thermal stability at 170°C can be explained by a combination of three effects.

Excessive epoxy ring-opening: At elevated curing temperatures, the ring-opening rate of epoxy groups exceeds 95%, which greatly increases molecular chain rigidity. Such rigidity reduces chain flexibility and facilitates

Table 4.—Thermal decomposition parameters of adhesives at different curing temperatures.

Curing temperature	Decomposition stage	Peak temperature (°C)	Weight loss (%)	Peak shape characteristics	Residual mass (%)
130°C	Primary decomposition	425 ± 2.1	$29.3 \pm 0.7$	Symmetrical single peak	$38.5 \pm 0.8$
170°C	Primary decomposition	$380 \pm 2.8$	$15.2 \pm 0.9$	Left-skewed broad peak	$41.7 \pm 1.2$
	Secondary decomposition	$450 \pm 3.5$	$12.8 \pm 0.7$	Right-skewed peak	_
Reference value	Sugarcane bagasse lignin	$295 \pm 1.5$	$60.2 \pm 1.2$	Sharp single peak	$28.3 \pm 0.6$

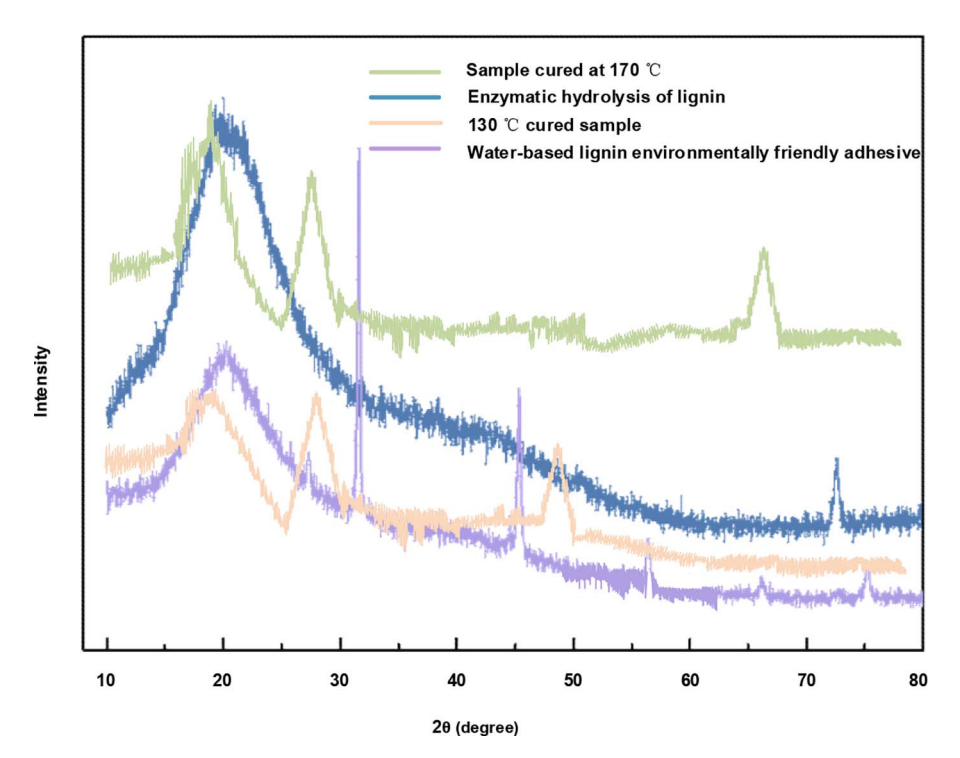


Figure 8.—Effect of thermal curing on the crystalline structure of the adhesive (from X-ray diffraction).

premature rupture of the polymer backbone, as reflected in the forward shift of the low-temperature degradation peak.

- Carbonization: Overcuring enhances the formation of a carbonized layer, which increases residual mass but simultaneously reduces mechanical toughness. The carbonized structures lack elasticity and may crack under stress, thereby limiting long-term reliability.
- 3. Loss of crystallinity: XRD demonstrated a 42% decrease in peak intensity and significant broadening of half-peak width, proving that high curing temperature destroys crystalline order. The loss of molecular alignment weakens the stability of the cross-linked network, making it more susceptible to thermal attack.

These three processes act synergistically, explaining the inferior thermal stability of adhesives cured at 170°C compared with those cured at moderate temperatures.

## Optimal curing window and performance implications

Considering the above results, curing at 130–150°C provides the best compromise between cross-linking efficiency and thermal stability. Within this window, the adhesive maintains high crystallinity, stable network structures, and reliable thermal resistance. However, when curing exceeds 160°C, irreversible network degradation occurs, crystallinity is lost, and flame-retardant performance declines, with the UL-94 rating decreasing from V-0 to V-1.

Future durability assessments should include accelerated aging tests (e.g., 85°C/85% relative humidity for 1,000 h), following procedures similar to ASTM G154 (ASTM, 2016), to quantitatively correlate the degree of crystallinity with performance retention over time.

Thermal decomposition kinetic parameters were calculated using the Kissinger equation, as shown in Equation 3.

$$Ln\left(\frac{\beta}{T_p^2}\right) = \frac{E_\alpha}{R} \cdot \frac{1}{T_p} + constant \tag{3}$$

where  $\beta$  is the heating rate (°C/min),  $T_p$  is the peak temperature (K), and  $E_a$  is the activation energy (kJ/mol).

The thermal decomposition kinetic parameters obtained from Equation (3) are summarized in Table 5. The results confirm that epoxy modification increases the activation energy by 64.5%, with the reaction order rising from 1.2 to 2.1, consistent with the three-dimensional cross-linked network decomposition mechanism.

Table 5. Thermal decomposition kinetic parameters of lignin-based adhesives.

Note:  $\beta$  = heating rate (°C/min);  $T_p$  = peak temperature (K);  $E_a$  = activation energy (kJ/mol). Reaction order (n) is derived from fitting decomposition data. Values represent the mean of three replicate tests.

In a 300°C constant-temperature ageing test (Figure 9), the optimized adhesive exhibited a mass retention rate of 78.5% after 72 hours, significantly outperforming commercial urea—formaldehyde resin (52.3%). Figure 9 further illustrates that the optimized epoxy-modified adhesive consistently maintains higher residual mass during prolonged

Table 5.—Thermal decomposition kinetic parameters.

Sample	T <sub>p</sub> (°C)	E <sub>a</sub> (kJ/mol)	Reaction order (n)
Sugarcane bagasse lignin	295	$98.7 \pm 3.2$	1.2
Optimized adhesive	425	$162.4 \pm 5.6$	2.1
Urea—formaldehyde resin (reference)	280	$85.3 \pm 2.8$	1.0

381

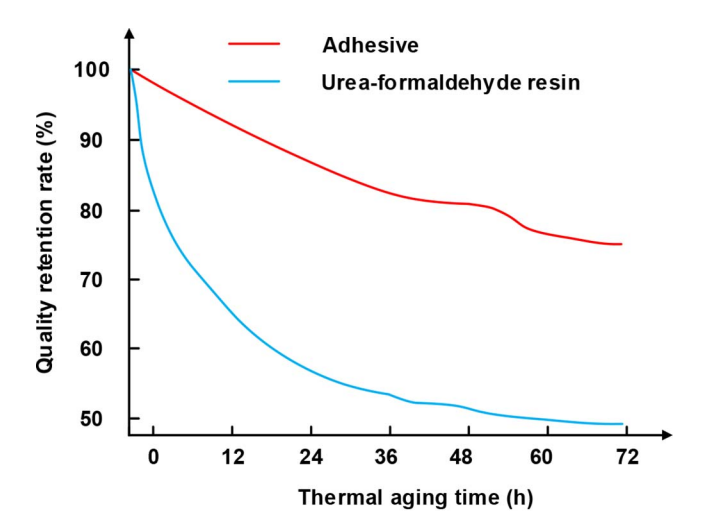


Figure 9.—300°C constant-temperature thermal ageing curve.

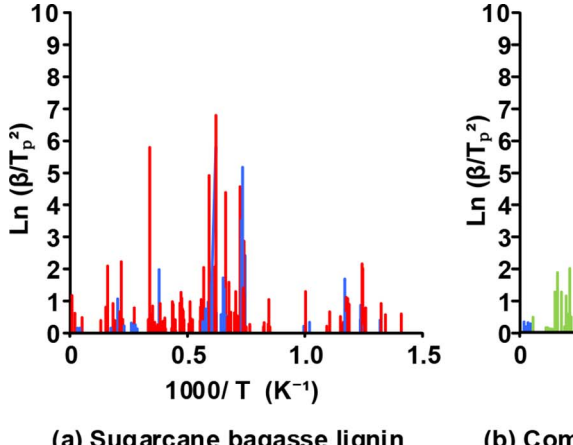
thermal exposure compared to conventional urea—formaldehyde and phenol—formaldehyde resins, highlighting its superior long-term thermal durability.

In Figure 9, the mass retention rates of the adhesive (red) and urea-formaldehyde resin (blue) are compared under a nitrogen atmosphere at 300°C. The shaded area indicates the inhibitory effect of the adhesive's cross-linked network on thermal oxidation. The adhesive (red curve) exhibits a three-stage decay characteristic: The initial 12-hour retention rate decreases gradually to 92.3 percent, primarily due to the evaporation of free water; during the middle stage (12 to 48 hours), the formation of the epoxy cross-linked network creates a physical barrier, reducing the weight loss rate to 0.21%/h and maintaining the retention rate at 82.1 percent; the later stage stabilizes, with a retention rate of 78.5 percent at 72 hours. The shaded area highlights the inhibitory effect of the cross-linked network on thermal oxidation, as its three-dimensional structure reduces free volume and hinders oxygen penetration. Additionally, the  $\beta$ -hydroxypropyl ether bond (bond energy 360 kJ/mol) provides superior chemical stability compared to the C-N bond in urea-formaldehyde resin. In contrast, urea-formaldehyde resin (blue curve) exhibits exponential degradation, losing 19.6 percent of its mass within the first 6 hours due to formaldehyde release and methylene bond breakage, with only 52.3 percent remaining after 72 hours. The high-temperature thermal stability of the adhesive stems from the synergistic effect between the aromatic ring conjugated system of lignin and the epoxy network. Its activation energy of 162.4 kJ/mol (Table 4) significantly delays molecular chain breakage, meeting the long-term reliability requirements of the 130°C to 150°C hot-pressing process for engineered wood panels.

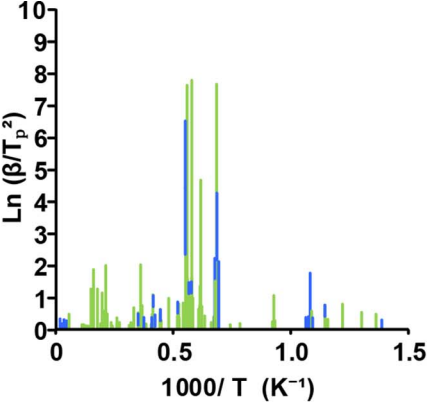
The high mass retention (78.5% after 72 hours at 300°C) and elevated activation energy (162.4 kJ/mol) demonstrated by this adhesive indicate exceptional resistance to thermal degradation. This property is critically beneficial for realworld applications where thermal cycling or fluctuating temperatures are common, such as in building materials exposed to diurnal temperature variations or automotive interiors. The stable, cross-linked network minimizes chain scission and volatile emission under periodic heating, thereby reducing internal stress buildup and preserving bond integrity over time. Compared to conventional urea-formaldehyde resin (52.3% retention), this lignin-based adhesive offers superior performance in environments requiring long-term thermal reliability. Future work will include specific thermal cycling tests (ASTM International, 1998, 2001, 2007) to quantitatively assess the retention of bonding strength after repeated exposure to cycles between  $-20^{\circ}$ C and  $120^{\circ}$ C, simulating extreme service conditions.

In Figure 10, the Arrhenius curves plotted using the Kissinger equation (Eq. 3) compare the thermal decomposition kinetics of the sugarcane bagasse lignin adhesive with those of commercial urea–formaldehyde resin. The x axis represents 1,000/T (K<sup>-1</sup>) (where T is the peak decomposition temperature), and the y axis represents  $\ln(\beta/T^2)$ , where  $\beta$  is the heating rate.

The data points for the sugarcane bagasse lignin epoxy adhesive are shown in red and exhibit high linear correlation ( $R^2 = 0.992$ ). The activation energy  $E_a$  was calculated from the slope of this linear relationship to be 162.4 kJ/mol (Table 4), which is significantly higher than the 85.3 kJ/mol for urea—formaldehyde resin. The higher distribution of the red data points indicates that, at the same temperature, the thermal decomposition rate constant of the sugarcane bagasse lignin adhesive is lower (e.g., the rate constant k at



(a) Sugarcane bagasse lignin adhesive



(b) Commercial urea formaldehyde resin

Figure 10.—Thermal decomposition Arrhenius curve.

FOREST PRODUCTS JOURNAL Vol. 75, No. 4

 $425^{\circ}$ C is  $1.58 \times 10^{-3} \text{ s}^{-1}$ , which is only 23% of that of urea-formaldehyde resin at 280°C). In contrast, the data points for urea-formaldehyde resin are blue, with a relatively gentle slope, yielding an activation energy  $E_a$  of 85.3 kJ/mol. In the low-temperature region (280°C to 300°C), the data points are more densely distributed, reflecting the rapid decomposition characteristics of urea-formaldehyde resin. For example, at  $300^{\circ}$ C, the rate constant k value of urea-formaldehyde resin reaches  $6.87 \times 10^{-3} \text{ s}^{-1}$ . differing by 334 percent from the k value of the adhesive at 425°C. As shown in Figure 10, sugarcane bagasse lignin adhesive exhibits higher thermal decomposition activation energy and lower thermal decomposition rate constants, indicating greater thermal stability at high temperatures. In contrast, ureaformaldehyde resin undergoes faster decomposition at lower temperatures, resulting in a higher thermal decomposition rate constant.

#### Conclusion

In the field of wood adhesives, the development of formaldehyde-free environmentally friendly materials holds significant application value. This study aimed to enhance the bonding performance and thermal stability of sugarcane bagasse lignin through epoxy modification, establishing a synthesis process system for green adhesives. An epoxy chloropropane grafting reaction was coupled with graded curing technology, and reaction parameters (temperature 90°C, lignin/ polyvinyl alcohol ratio 1:1. NaOH addition 15 mL) were optimized via orthogonal experiments. Performance characterization was conducted using XRD, TGA, and bonding strength testing. Experimental data showed that under the optimized process, the adhesive strength reached 2.72  $\pm$ 0.15 MPa, exceeding the national standard of 0.7 MPa by 288 percent; the thermal decomposition activation energy increased to  $162.4 \pm 5.6$  kJ/mol, representing a 64.5 percent increase compared to unmodified lignin; and after 72 hours of thermal ageing at 300°C, the mass retention rate was 78.5 percent, i.e., significantly better than that of ureaformaldehyde resin (52.3%). XRD analysis showed that the crystallization peak intensity of the 130°C cured sample was 12,546 a.u., while overcuring at 170°C caused a 42 percent decrease in crystallization intensity. The study's contribution lies in revealing the temperature-sensitive mechanism: 160°C is the curing critical point at which the epoxy group conversion rate reaches 92.4 percent, and the UL-94 flame retardant rating remains V-0; above 160°C, the cross-linked network degrades, the flame retardant rating drops to V-2, and the water absorption expansion rate reaches 9.7 percent (exceeding the national standard upper limit of 8.0%). At high-temperature curing, the temperature difference between the two decomposition peaks expanded to 85°C, and the structural stability of the residual carbon layer decreased. The main limitation is that material testing was focused on pine wood substrates and did not cover hardwood or composite materials. Future research will expand to validate the suitability of substrates such as oak and bamboo fiber, develop an in-situ silane dynamic cross-linking system to suppress high-temperature expansion, and design a ±2°C precision temperature-controlled reactor combined with infrared online monitoring to enhance process stability. While this study successfully demonstrated the high performance of the optimized adhesive on pine wood (a softwood representative), the investigation of its compatibility with a broader range of substrates is indeed a critical next step for practical applicability. Future studies are explicitly planned to expand the testing to include hardwoods (e.g., oak, eucalyptus) and engineered composite panels (e.g., bamboo fiber-reinforced composites, particleboards). This expansion will validate the universality of the adhesion mechanism and assess interface adaptability across different surface chemistries and morphologies. Collaborations with industrial partners are being established to evaluate performance under real-world manufacturing conditions. The results of this research provide technical support for the industrialization of sugarcane bagasse resource utilization and formaldehyde-free engineered wood panels.

## Acknowledgment

This work was supported by the Basic Research Ability Improvement Project of Young and Middle-Aged Teachers of Guangxi Universities (2023KY0880).

#### Literature Cited

- Aldroubi, S., M. El-Sakhawy, S. Kamel, P. Hesemann, A. Mehdi, and N. Brun. 2023. Ionothermal carbonization of sugarcane bagasse in imidazolium tetrachloroferrate ionic liquids: Effect of the cation on textural and morphological properties. *Green Chem.* 25(9):3533–3542. https://doi.org/10.1039/D3GC00300K
- Amiripour, F., S. Ghasemi, and M. J. Chaichi. 2024. Nanostructured rhodamine B/aluminosilicate extracted sugarcane bagasse modified with tobacco-derived carbon quantum dot as ratiometric fluorescence probe for determination of tetracycline. *Talanta* 276:126158. https://doi.org/ 10.1016/j.talanta.2024.126158
- ASTM 1998: ASTM D905-98. Standard Test Method for Strength Properties of Adhesive Bonds in Shear by Compression Loading. ASTM International, West Conshohocken, PA, 1998.
- ASTM 2001. ASTM D906-98 (Reapproved 2001). Standard Test Method for Strength Properties of Adhesives in Plywood Type Construction by Shear in Tension Loading. ASTM International, West Conshohocken, PA, 2001.
- ASTM 2007: ASTM D5751-99 (Reapproved 2007). Standard Practice for Evaluating Performance of Structural Wood Adhesives for Use Under Exterior Exposure Conditions. ASTM International, West Conshohocken, PA, 2007.
- Buarque, F. S., C. E. C. D. Souza, R. M. Ferreira, T. O. Sabino, O. M. J. Teixeira, L. F. M. Bandeira, A. C. Fraga, M. A. Z. Coelho, and B. D. Ribeiro. 2024. Dissolution and enzymatic hydrolysis of sugarcane bagasse using ionic liquids and deep eutectic solvents. *Process Biochem.* 147:257–267. https://doi.org/10.1016/j.procbio.2024.08.024
- Castanheira, J. D. P., J. H. R. Llanos, J. R. Martins, M. L. Costa, and M. Brienzo. 2025. Acetylated xylan from sugarcane bagasse: Advancing bioplastic formation with enhanced water resistance. *Polym. Bull*. 82(5):1705–1722. https://doi.org/10.1007/s00289-024-05597-z
- Chen, Y. X., H. S. Zhu, F. Gao, H. R. Xiong, H. Yang, Z. X. Xu, P. G. Duan, L. J. Zheng, S. M. Osman, and R. Luque. 2024. Green wood bio-adhesives from cellulose-derived bamboo powder hydrochars. *Chem. Eng. J.* 498:155667. https://doi.org/10.1016/j.cej.2024.155667
- Cheon, H., J. H. Kim, J. S. Kim, and J. B. Park. 2024. Valorization of single-carbon chemicals by using carboligases as key enzymes. *Curr. Opin. Biotechnol.* 85:103047. https://doi.org/10.1016/j.copbio.2023. 103047
- Cho, S. H., J. Park, D. Lee, H. Cho, J. Lee, and E. E. Kwon. 2024. Recovery of gaseous fuels through  $\rm CO_2$ -mediated pyrolysis of thermosetting polymer waste. *Chemosphere* 363:142892. https://doi.org/10.1016/j.chemosphere.2024.142892
- Du, Y., Y. Zhu, J., Li, Y. Li, and J. Xiao. 2024. Multifunctional superhydrophobic sugarcane bagasse capable of efficiently separating oil—water mixtures and degrading MB. *Int. J. Biol. Macromol.* 283(Pt.1):137386. https://doi.org/10.1016/j.ijbiomac.2024.137386

- Ghahri, S., E. S. Wibowo, and B. D. Park. 2024. Crosslinking reactions of a model aminated lignin compound as a platform for building thermosetting polymers for lignin-based bio adhesives. *Bioresour. Tech*nol. 413:131500. https://doi.org/10.1016/j.biortech.2024.131500
- He, Y., T. Liu, and Y. Deng. 2025. Enhanced norfloxacin removal by eco-friendly MgFe<sub>2</sub>O<sub>4</sub> modified sugarcane bagasse biochar: Adsorption performances and mechanisms. *New J. Chem.* 49(9):3783–3794. https://doi.org/10.1039/D4NJ05076B
- ISO 2008: ISO 291:2008. Plastics Standard Atmospheres for Conditioning and Testing. International Organization for Standardization, Geneva, Switzerland, 2008.
- Lin, Y. R., M. W. Zheng, and S. H. Liu. 2023. Silica wastes derived multifunctional coatings for formaldehyde photodegradation and autonomous indoor humidity buffering. *Chemosphere* 341:140118. https://doi.org/10.1016/j.chemosphere.2023.140118
- Lubis, M. A. R., F. Falah, D. Harini, Sudarmanto, A. Kharisma, B. Tjahyono, W. Fatriasari, B. Subiyanto, L. Suryanegara, and A. H. Iswanto. 2023. Enhancing the performance of natural rubber latex with polymeric isocyanate as cold-pressing and formaldehyde free adhesive for plywood. *J. Adhes.* 9(1–4):58–73. https://doi.org/10.1080/00218464.2021.1999233
- Mauri, S., R. Calligaro, C. F. Pauletti, M. F. Camellone, M. Boaro, L. Braglia, S. Fabris, S. Piccinin, P. Torelli, and A. Trovarelli. 2024. Low-temperature methane activation reaction pathways over mechanochemically-generated Ce<sup>4+</sup>/Cu interfacial sites. *Small* 20(42):2403028. https://doi.org/10.1002/smll.202403028
- Meng, T., Y. Ding, Y. Liu, L. Xu, Y. Mao, J. Gelfond, S. Li, Z. Li, P. F. Salipante, H. Kim, J. Y. Zhu, X. Pan, and L. Hu. 2023. In situ lignin adhesion for high-performance bamboo composites. *Nano Lett.* 23(18):8411–8418. https://doi.org/10.1021/acs.nanolett.3c01497
- Pan, J., Y. Li, and M. Zhang. 2024. Bio-based Epoxy Resin Systems Derived from Lignin for Sustainable Wood Adhesives. Industrial Crops and Products, 215, 118908.
- Siahkamari, M., D. Debnath, T. Wang, and M. Nejad. 2025. A fundamental study of lignin reactions with formaldehyde and glyoxal. *Green Chem.* 27(8):2342–2358. https://doi.org/10.1039/d4gc05695g
- Soliman, M., M. Wageed, S. Alsherbeny, S. Safty, Y. Su, A. M. Ali, and R. Sayed. 2022. Sugarcane bagasse as low-cost solid-phase extraction sorbent for pesticides in water. *Int. J. Environ. Anal. Chem.* 104(18):6324— 6338. https://doi.org/10.1080/03067319.2022.2142048
- Song, G., D. Liu, M. Madadi, L. Liu, C. Li, Q. Liu, C. Sun, E. Zhang, A. Ashori, and F. Sun. 2025. Surfactant-aided acid glycerol pretreatment

- of sugarcane bagasse: Dual benefits of substrate and lignin modifications for improved enzymatic hydrolysis. *Energy* 320:135520. https://doi.org/10.1016/j.energy.2025.135520
- Standardization Administration of China. 2004. GB/T 9846-2004. Plywood for general use. Beijing, China.
- Standardization Administration of China 2013; Standardization Administration of China. (2013). GB/T 9846-2013: Plywood. Beijing: Standards Press of China.
- Sunar, S. L., D. Bhattacharyya, D. Shee, and T. K. Panda. 2025. Efficient fractionation of sugarcane bagasse to bio-based building blocks using a tailored deep eutectic solvent and process optimization. Waste Biomass Valorization. Published online 24 March 2025. https://doi.org/ 10.1007/s12649-025-03019-3
- Xu, Z. X., H. R. Xiong, R. Dou, Y. Tan, Y. X. Chen, and L. J. Leng. 2024. Hydrochar-based facile and green wood bio-adhesives production from distilled spent grain. *Chem. Eng. J.* 481:148694. https://doi. org/10.1016/j.cej.2024.148694
- Yue, Z., G. Lu, W. Wei, Y. Huang, Z. Chen, F. Dingwall, S. Shao, and X. Fan. 2024. Engineered half-unit-cell  $MoS_2/ZnIn_2S_4$  monolayer photocatalysts and adsorbed hydroxyl radicals-assisted activation of  $C\alpha$ -H bond for efficient  $C\beta$ -O bond cleavage in lignin to aromatic monomers. ACS Appl. Mater. Interfaces 16(36):47724–47740. https://doi.org/10.1021/acsami.4c10515
- Zhang, X., C. Long, X. Zhu, X. Zhang, J. Li, J. Luo, J. Li, and Q. Gao. 2023. Preparation of strong and thermally conductive, spider silkinspired, soybean protein-based adhesive for thermally conductive wood-based composites. ACS Nano 17(19):18850–18863. https://doi. org/10.1021/acsnano.3c03782
- Zhao, H., W. Yao, G. Liu, J. Wang, J. Li, and Q. Gao. 2024. A new strategy for the preparation of high-strength hydrophobic aldehyde-free starch adhesive. *Polym. Adv. Technol.* 35(12):e7000–e7011. https://doi.org/10.1002/pat.70000
- Zhao, J., H. Wang, Y. Kan, G. Liu, J. Wang, J. Li, and Q. Gao. 2025. A synergistic strategy for cost-effectively reducing formaldehyde emission of urea-formaldehyde resin via glyoxal copolymerization and urea post-addition. *J. Appl. Polym. Sci.* 142(16):e56750. https://doi. org/10.1002/app.56750
- Zuo, H., and Z. Liu. 2023. Thermal and structural analysis of the reaction mechanisms during the preparation of activated carbon from sugarcane bagasse by urea phosphate activation. *Cellulose* 31(2):793–808. https://doi.org/10.1007/s10570-023-05622-w